ON MAPPING FUNCTIONS FOR TORSIONAL ANALYSIS OF SPLINED SHAFTS

By Kwan Rim[1] and Louis Camillo[2]

Abstract[3]

33191

The purpose of this paper is to introduce a practical method of deriving relatively simple mapping functions, which are needed in the torsional analysis of splined shafts. The form of the mapping functions being simple, it is shown that the analytical solutions are readily obtainable without undue labor, and that an approximate but systematic analysis of any splined shaft is now possible. The mapping functions are also capable of analyzing splined shafts with very sharp re-entrant corners, which would not only defy the known methods of numerical analysis but also present some difficulties to experimental methods of analysis. Torsional analysis of a typical splined shaft is carried out; and the experimental errors associated with sharp re-entrant corners are illustrated through a carefully conducted experiment.

Author

1. Associate Professor, Department of Mechanics and Hydraulics, University of Iowa, Iowa City, Iowa

2. Engineer, Materials Engineering Department, Deere & Company, Moline Illinois

3. This paper includes research efforts supported by National Aeronautics and Space Administration, under NsG-576

Notation

i	$\sqrt{-1}$
z, ζ	Complex numbers; i.e., $z = x + iy$
$\bar{z}$, $\bar{\zeta}$	Conjugate of complex numbers; i.e., $\bar{z} = x - iy$
$f(\zeta)$	Mapping function
n	Number of notches
j, k, l, m	Indices
K_j	Exterior angle of the j-th vertex divided by π
a_j, b_j, ...	Images of vertices on the unit circle
γ_j	Spacing of images on the unit circle
τ	Resultant shear stress
τ_{zx}, τ_{zy}	Components of shear stress in the x- and y-directions, respectively
ϕ	Warping function
J	Torsional constant
T	Torque applied at the ends of the prismatic bar
K	Stress concentration factor
∇^2	Laplace's operator
W	Lateral displacement of membrane
p	Lateral pressure on membrane (psi)
F	Tension force in the uniformly stretched membrane (lbs/in.)
V	Volume under the distended membrane
$(\ )'$	$\frac{\partial}{\partial\zeta}(\ )$

Introduction

It is well known that the function mapping a circle onto a simple region with n axes of symmetry has the general form [1]*

$$z = f(\zeta) = \sum_{m=0}^{\infty} C_m \zeta^{1+nm}, \quad C_m = \overline{C}_m. \tag{1}$$

However, an application of a mapping function expressed in an infinite series is prohibitive. The usual approach is to form an approximate polynomial mapping function which is obtained by truncating the infinite series after a certain term. The desirable characteristics of such an approximate mapping function are: reasonable congruency of the mapped to the specified region and simplicity of the mapping function. The significance of congruency is self-evident and does not require any further explanation. Simplicity also becomes very important, since a complicated mapping function te s to diminish the merits of analytic solutions. As the complexity of an analytic solution increases, so does the difficulty of comprehending its physical implications. It should be noted that the numerical answers provided by a complicated analytic solution may as well be obtained, with less computational effort, by using some reliable numerical method.

There exist several different methods of constructing approximate mapping functions; e.g., Melentiev's method [2]. Most of these methods, however, yield polynomials with a very large number of terms (several dozen to a few hundred) for a reasonably congruent mapping of a star-

---

* Numbers in brackets designate references at the end of paper.

shaped region. A careful review of various mapping techniques showed that a proper application of the well-known method of the Schwarz-Christoffel transformation (see [3] for an extensive list of references) offered several advantages, particularly in the case of splined shaft analyses.

The first advantage is simplicity of the method: the coefficients of the power series are automatically determined and remain fixed, and they are directly related to the physical parameters controlling the size and shape of the shaft cross section. The second advantage is that, compared to other methods, it usually yields polynomials with a smaller number of terms for the same degree of mapping accuracy. It is also capable of mapping the cross section of a splined shaft with sharp re-entrant corners. Appropriate polynomials are derived by examining the congruency and truncating the series according to a desired accuracy. Another point of great significance is that all the polynomials obtained through truncation do automatically satisfy the condition of conformality.

Most of the other methods of approximate conformal transformation do not possess these properties. In many cases, the coefficients of a polynomial mapping function must be re-evaluated for every new approximation; and some methods require one to start with an enormously large number of terms in order to ensure that the condition of conformality will be satisfied.

Derivation of Mapping Functions

The general formula for the conformal mapping of the interior of a unit circle onto the interior of a closed polygon [4] is given by

$$z = f(\zeta) = A\int_0^{\zeta} (\zeta_1 - \zeta)^{-K_1}(\zeta_2 - \zeta)^{-K_2}\ldots(\zeta_n - \zeta)^{-K_n}d\zeta, \quad (2)$$

in which A is a complex constant and K_j is related to the exterior angle of the polygon at its vertex z_j by the factor of π. It may appear that an application of the Schwarz-Christoffel transformation is likely to result into a sort of intractable complication in the case of a polygon with many sides. However, it turns out that the approximate mapping of the cross sections of usual splined shafts can be transacted without much difficulty, since they may be closely approximated by relatively simple polygons with high degree of symmetry.

Consider a shaft whose cross section may be well approximated by a simple star shown in Figure 1. The mapping function is given by

$$z = f(\zeta) = A\int_0^{\zeta} (1 + \zeta^n)^{k_2}(1 - \zeta^n)^{-k_1}d\zeta, \quad (3)$$

which results directly from the general equation (2). Although the integral cannot be evaluated in terms of elementary functions, one may

a) Expand the integrand into a power series

b) Integrate the series term by term

c) Derive an approximate mapping function in the form of a polynomial which is obtained by truncating the series at an appropriate place.

In such a manner, the following polynomial is obtained from Eq. (3):

$$z = f(\zeta) = A[\zeta + C_1\zeta^{n+1} + C_2\zeta^{2n+1} + \ldots + C_m\zeta^{mn+1}], \quad (4)$$

in which

$$C_1 = \frac{1}{n+1}(K_1 + K_2),$$

$$C_2 = \frac{1}{2n+1}\left[\frac{K_2(K_2-1)}{2!} + K_1K_2 + \frac{K_1(K_1+1)}{2!}\right],$$

$$C_3 = \frac{1}{3n+1}\left[\frac{K_2(K_2-1)(K_2-2)}{3!} + \frac{K_1K_2(K_1+K_2)}{2!} + \frac{K_1(K_1+1)(K_1+2)}{3!}\right],$$

. . . .

This agrees with the general expression given by Eq. (1). Eq. (4) contains the well-known mapping function

$$z = f(\zeta) = A(\zeta + C_1\zeta^{n+1}), \tag{5}$$

which was used by Stevenson [5] in this torsional analysis of a fluted column. The coefficient C_1 of Eq. (5) controls the spline depth. However, it is bounded by the conformality condition in such a way that Eq. (5) is not capable of mapping a cross section with sufficient spline depth.

The fewer the number of terms retained in the polynomial, Eq. (4); the less accurate the mapping becomes. However, it is observed that a polynomial with a relatively small number of terms can often accomplish a reasonably accurate mapping. See Figure 2. In general, the effect of truncation is that of mapping a figure nearly congruent to the prescribed polygon but with rounded corners. Another interesting observation is that, if a polynomial is generated from a deep star (large K_1) and only a very few terms (3 to 4) are retained, it maps a figure closely resembling some of the involute spline profiles. See Figure 3.

It is also possible to improve the accuracy of mapping by merely adjusting the numerical coefficients of a given polynomial; namely, without increasing the number of terms in the polynomial [6]. However, the extent of such adjustment is limited by the condition of conformality. Since all the approximate mapping functions are being derived in the form of polynomials, the condition of conformality may be simply stated that all the roots of a polynomial, corresponding to the derivative of a mapping function, must lie on the exterior of a unit circle.

Derivation of mapping functions from Eq. (3) is simple, but their usefulness is limited to the analyses of serrated shafts and a certain kind of splined shaft shown in Figure 2 and Figure 3, respectively. In order to generate mapping functions for a very large class of splined shafts, the polygon shown in Figure 4 is considered. Proper substitution and regrouping of terms in Eq. (2) reduces the mapping function for such a polygon to

$$z = A'\int_0^{\zeta}\frac{[(d_1-\zeta)\ldots(d_n-\zeta)]^{K_3}[(c_1-\zeta)\ldots(c_n-\zeta)]^{K_2}[(e_1-\zeta)\ldots(e_n-\zeta)]^{K_2}}{[(a_1-\zeta)\ldots(a_n-\zeta)]^{K_0}[(b_1-\zeta)\ldots(b_n-\zeta)]^{K_1}[(f_1-\zeta)\ldots(f_n-\zeta)]^{K_1}}\,d\zeta, \qquad (6)$$

in which a_j, b_j, ... f_j are defined by

$$a_1 = e^{i\theta},\ b_1 = e^{i\gamma_1},\ c_1 = e^{i\gamma_2},\ d_1 = e^{i\frac{\pi}{n}},\ e_1 = e^{i(\frac{2\pi}{n} - \gamma_2)},\ f_1 = e^{i(\frac{2\pi}{n} - \gamma_1)}$$

and by the general relationship

$$\beta_j = \beta_1 e^{i\frac{2\pi}{n}(j - 1)},\quad \beta_j = a_j, b_j, \ldots, f_j;\ (j = 1, 2, \ldots n).$$

It can be shown that

$$(\beta_1 - \zeta)(\beta_2 - \zeta)\ldots(\beta_n - \zeta) = \prod_{j=1}^{n}\left[\beta_1 e^{i\frac{2\pi}{n}(j-1)}\right] = \beta_1^n - \zeta^n.$$

Thus, observing that a_n and d_n correspond to the n-th roots of +1 and -1, respectively, Eq. (6) reduces to

$$z = A\int_0^{\zeta}\frac{(1 + \zeta^n)^{K_3}[(1 - e^{-in\gamma_2}\zeta^n)(1 - e^{in\gamma_2}\zeta^n)]^{K_2}}{(1 - \zeta^n)^{K_0}[(1 - e^{-in\gamma_1}\zeta^n)(1 - e^{in\gamma_1}\zeta^n)]^{K_1}}\,d\zeta. \qquad (7)$$

Derivation of approximate functions from Eq. (7) is the same as the preceding case of a simple polygon, except for somewhat increased complexity of expanding the integrand. A systematic expansion of the integrand may be carried out by expanding each parenthesized quantity and then forming the product of all the series. For example, an expansion of the quantity

$$[(1 - e^{-in\gamma_j}\zeta^n)(1 - e^{in\gamma_j}\zeta^n)]^{K_j} \qquad (j = 1, 2)$$

may be carried out in the following manner:

$$(1 - e^{-in\gamma_j}\zeta^n)^{K_j} = 1 + \sum_{k=1}^{\infty}\left[\prod_{m=0}^{k-1}(K_j - m)\right]\frac{e^{-in\gamma_j k}(-\zeta^n)^k}{k!} = \sum_{k=0}^{\infty} A_k\zeta^{nk},$$

$$(1 - e^{in\gamma_j}\zeta^n)^{K_j} = 1 + \sum_{k=1}^{\infty}\left[\prod_{m=0}^{k-1}(K_j \quad m)\right]\frac{e^{in\gamma_j k}(-\zeta^n)^k}{k!} = \sum_{k=0}^{\infty} B_k\zeta^{nk};$$

hence,

$$[(1 - e^{-in\gamma_j}\zeta^n)(1 - e^{in\gamma_j}\zeta^n)]^{K_j} = \sum_{k=0}^{\infty} C_k(\gamma_j, K_j)\zeta^{nk} \tag{8}$$

where the coefficients $C_k(\gamma_j, K_j)$ are defined by

$$C_k(\gamma_j, K_j) = \sum_{\ell=0}^{k} A_\ell B_{k-\ell},$$

i.e.,

$$C_0(\gamma_j, K_j) = 1, \quad C_1(\gamma_j, K_j) = -K_j 2\cos(n\gamma_j),$$

$$C_2(\gamma_j, K_j) = \frac{K_j(K_j - 1)}{2!}\, 2\cos(2n\gamma_j) + K_j K_j,$$

$$C_3(\gamma_j, K_j) = \frac{-K_j(K_j - 1)(K_j - 2)}{3!}\, 2\cos(3n\gamma_j) - \frac{K_j}{1!}\frac{K_j(K_j - 1)}{2!}\, 2\cos(n\gamma_j),$$

$$C_4(\gamma_j, K_j) = \frac{K_j(K_j - 1)(K_j - 2)(K_j - 3)}{4!}\, 2\cos(4n\gamma_j) + \frac{K_j}{1!}\frac{K_j(K_j - 1)(K_j - 2)}{3!}\, 2\cos(2n\gamma_j) + \left[\frac{K_j(K_j - 1)}{2!}\right]^2,$$

. . . .

Thus, Eq. (7) may now be expressed in terms of the products of the series defined by Eq. (8)

$$z = A\int_0^{\zeta}\left[\sum_{k=0}^{\infty} C_k(\frac{\pi}{n}, \frac{K_3}{2})\zeta^{nk}\right]\left[\sum_{k=0}^{\infty} C_k(0, \frac{-K_0}{2})\zeta^{nk}\right] \tag{9}$$

$$\times\left[\sum_{k=0}^{\infty} C_k(\gamma_2, K_2)\zeta^{nk}\right]\left[\sum_{k=0}^{\infty} C_k(\gamma_1, -K_1)\zeta^{nk}\right] d\zeta,$$

which becomes

$$z = A\int_0^{\zeta}\left[\sum_{k=0}^{\infty} D_k(\gamma_1, \gamma_2, K_1, K_2, K_3)\zeta^{nk}\right] d\zeta. \tag{10}$$

In Eq. (10), the series $\sum_{k=0}^{\infty} D_k\zeta^{nk}$ is the final product of the series constituting the integrand of Eq. (9). Coefficients D_k are determined by a computer through an available subroutine for power series multiplication. Final form of the mapping function is given by

$$z = A\sum_{k=0}^{\infty} \frac{D_k}{1 + nk}\,\zeta^{1+nk}, \tag{11}$$

which again agrees with the general expression, Eq. (1).

An approximate mapping function may be derived by truncating either the final series (11) or each of the four series in Eq. (9) at appropriate places. The latter procedure offers certain advantages, if one makes use of the following facts. Each of the four series is determined uniquely by the properties of a particular vertex of the polygon; namely, each series corresponds to a particular vertex, and the mapping of the vicinity of a vertex is primarily controlled by the corresponding series. In other words, the more terms that are retained in the corresponding polynomial, the more accurate the mapping of a particular vertex region becomes, and vice versa. Furthermore, for the same accuracy of mapping, the polynomial corresponding to a vertex with a negative exterior angle requires fewer terms than one with a positive exterior angle. The exterior angle of the polygon at a vertex is measured positive in the counter-clockwise direction.

The figure mapped by Eq. (11) is controlled by three types of parameters. They are the normalizing coefficient A, the factors relating to the exterior vertex angles (K_1, K_2, K_3), and the spacing of the vertex images on the unit circle $(\gamma_1$ and $\dot{\gamma}_2)$. The normalizing coefficient A is determined in such a way that the distance from the center to the outer tip of a polygon is a unity and that one of the polygon's major axes of symmetry is oriented along the x-axis. It may be readily evaluated by letting $z = 1$ be the image of $\zeta = 1$; i.e.,

$$1 = A \sum_{k=0}^{\infty} \frac{D_k}{1 + nk} .$$

Instead of normalizing, one may also determine A directly to match the mapped figure with the spline cross section. The exterior angles are of course known from a given polygon. The proper spacing of the vertex images is determined from the relative side dimensions of the polygon, by following a procedure similar to that in [7]. Samples of mapping functions generated from the type of polygon shown in Figure 4 are plotted in Figures 5 and 6. Reasonably accurate mappings of typical involute spline cross sections are accomplished by polynomials with a small number of terms.

Stress Analysis

Since the formal solution of a prismatic bar subjected to a pure torsion is available in a number of excellent standard texts [8] [9], the final results will be used without derivation. The torsional constant and the components of shear stress are given as follows [9]:

$$J = \frac{1}{4i}\oint_{S_1} [\overline{f}(\overline{\zeta})]^2 f(\zeta)f'(\zeta)d\zeta$$
$$- \frac{1}{4}\oint_{S_1} [F_1(\zeta) + \overline{F}_1(\overline{\zeta})][f(\zeta)d\overline{f}(\overline{\zeta}) + \overline{f}(\overline{\zeta})df(\zeta)], \qquad (12)$$

$$\tau_{zx} - i\tau_{zy} = \frac{T}{J}\left[\frac{F_1'(\zeta)}{f'(\zeta)} - i\overline{f}(\overline{\zeta})\right], \qquad (13)$$

in which $f(\zeta)$ is a mapping function and $F_1(\zeta)$ is an analytic function defined by

$$F_1 = \sum_{m=1}^{\infty}\left(i\sum_{k=-\infty}^{\infty} A_{m+k}\overline{A}_k\right)\zeta^m \qquad (14)$$

where

$$A_m = \frac{1}{2\pi}\int_0^{2\pi} f(\zeta)e^{-im\theta}d\theta, \qquad \text{on } |\zeta| = 1.$$

As an example, let us consider a mapping function which is a simple three-term polynomial:

$$z = f(\zeta) = A(\zeta + C_1\zeta^{n+1} + C_2\zeta^{2n+1}). \qquad (15)$$

Then, eqs. (14), (12), and (13) may be expressed in terms of the coefficients of the mapping function as follows:

$$F_1(\zeta) = iA^2[C_1(1 + C_2)\zeta^n + C_2\zeta^{2n}],$$

$$J = \pi A^4[\tfrac{1}{2}(1 - C_2^4) + 2(C_1^2 + C_2^2 + C_1^2C_2)$$
$$+ (n + 1)(\tfrac{1}{2}C_1^4 + C_2^4 + 2C_1^2C_2^2)], \qquad (16)$$

$$\tau_{zx} - i\tau_{zy} = \frac{iAT}{J}\left[\frac{nC_1(1 + C_2)\zeta^{n-1} + 2nC_2\zeta^{2n-1}}{1 + (n + 1)C_1\zeta^n + (2n + 1)C_2\zeta^{2n}} - \bar{\zeta} - C_1(\bar{\zeta})^{+1}\right.$$
$$\left. - C_2(\bar{\zeta})^{2n+1}\right]. \qquad (17)$$

As a specific numerical example, let us investigate a 12-notch splined shaft with major and minor radii of 1.493 in. and 1.292 in., respectively, by using one of the mapping functions presented in Figure 3. The mapping function

$$z = f(\zeta) = 1.357(\zeta + 0.07\zeta^{13} + 0.03\zeta^{25}) \qquad (18)$$

is simple but transacts the conformal mapping of a figure which is reasonable close to a splined shaft cross section. The radius of fillet is only 0.00277 in. representing a sharp re-entrant corner. Substituting the coefficients of the mapping function (18) into Eqs. (16) and (17), the torsional constant and the shear stress are obtained as follows:

$$J = 5.453 \text{ (in.)}^4,$$

$$\tau_{zx} - i\tau_{zy} = 0.2488iT\left[\frac{4.6525\zeta^{11} + 0.72\zeta^{23}}{1 + 0.91\zeta^{12} + 0.75\zeta^{24}} - \bar{\zeta} - 0.07(\bar{\zeta})^{13} - 0.03(\bar{\zeta})^{25}\right],$$

$$\tau = \sqrt{\tau_{zx}^2 + \tau_{zy}^2} \quad .$$

The plot of the shear stress distribution is presented in Figure 7. At the point of the maximum shear stress, $z = f(e^{i\frac{\pi}{18}})$, we have

$$\tau_{zx} - i\tau_{zy} = 0.2488T(-3.316 - i\ 2.858),$$

and the maximum resultant shear stress is given by

$$\tau_{max} = 0.2488T\sqrt{(3.316)^2 + (2.858)^2} = 1.09\ T \text{ psi}.$$

Since the maximum shear stress of a circular cylinder with the minimum radius of the splined shaft is given by

$$\tau'_{max.} = \frac{2T}{\pi (R_{min.})^3} = \frac{2T}{\pi (1.292)^3} = 0.296T \text{ psi.},$$

the stress concentration factor is found to be

$$K = \frac{1.09\ T}{0.296\ T} = 3.68.$$

Experimental Analysis

Since the sharp geometric changes in the cross section might introduce considerable errors to the results of any numerical analysis and even to the experimental results, the authors have conducted a very careful experimental analysis using the membrane analogy technique. Hence, the purpose of the experiment is to investigate the accuracy of the experimentally evaluated stress concentration factors, especially in the case of a splined shaft with sharp re-entrant corners.

The membrane used in the experiment is a latex rubber sheet with the thickness of 0.007 in. and the elastic elongation of at least 200 percent. Measurement of the elevation of the deflected membrane is greatly facilitated by applying an aqueous solution of potasium dichromate on the membrane. Any contact between the micrometer probe and the conducting membrane surface is immediately detected by a sensitive galvanometer. The volume covered by the deflected membrane and the slope of the membrane at any point are calculated from the readings of the membrane elevation. The formulas for the torsional constant and the shear stress [10] are given by

$$J = 4 \frac{F}{p} V, \tag{19}$$

$$\tau = - \frac{T}{2V} \frac{\partial W}{\partial N}, \tag{20}$$

in which the F/P ratio can be determined by measuring the elevation of the membrane at the center of the circular test hole [10]:

$$\frac{P}{F} = \frac{4}{r_a^2} z_0 \; . \tag{21}$$

In Eq. (21), r_a is the radius of the test hole and z_0 is the elevation of the membrane at the center of the test hole.

The experimental results are presented in Table 1 along with the theoretical values.

	$\dot{V}$ (Volume)	J (Exp.)	J (Theo.)	Max. (Exp.)	Max. (Theo.)
Theoretical Splined Shaft	0.295	5.23	5.45	0.93T	1.09T

Table 1. Experimental Results

In spite of very carefully repeated experimentations, it is observ d that the experimental value of the maximum shear stress has a somewhat large error of -14.7 percent. Based on this investigation, it appears the experimentally evaluated stress concentration factors should be reviewed rather carefully.

Conclusions

The success of the complex variable method in elasticity hinges upon the availability and simplicity of a mapping function. Although the existence of such a mapping function is guaranteed by the celebrated mapping theorem of Riemann [11], means for the actual construction of arbitrary mapping functions have not been devised. The authors have shown that the approximate mapping of the cross sections of splined shafts may be readily transacted through a proper application of the Schwarz-Christoffel transformation. It is due to the fact that the cross sections may be closely approximated by relatively simple polygons with high degrees of symmetry.

Compared to other methods of approximate conformal transformations, the present method does provide a simple mapping function for the analysis of a splined shaft and it offers some unique advantages. Some of the advantages are: unique and automatic determination of the coefficients of the mapping function, automatic satisfaction of the conformality condition, and the simple geometric interpretation of the parameters which control the coefficients. The form of the mapping functions being simple, it is now possible to accomplish an approximate but systematic analysis of any splined shafts without undue labor.

The stress concentration factor of 3.68, found for the particular splined shaft considered for the numerical example, is higher than the available analytical results of similar shafts [12][13]. This is due to the fact that the present analysis dealt with a shaft with a smaller fillet radius, which is more typical of the splined shafts used by industry.

Acknowledgment

The authors wish to thank Professor Miklós Hetényi, Stanford University, for his kindness in reviewing the manuscript and making valuable suggestions, and Deere & Company for their support of the experimental work contained herein.

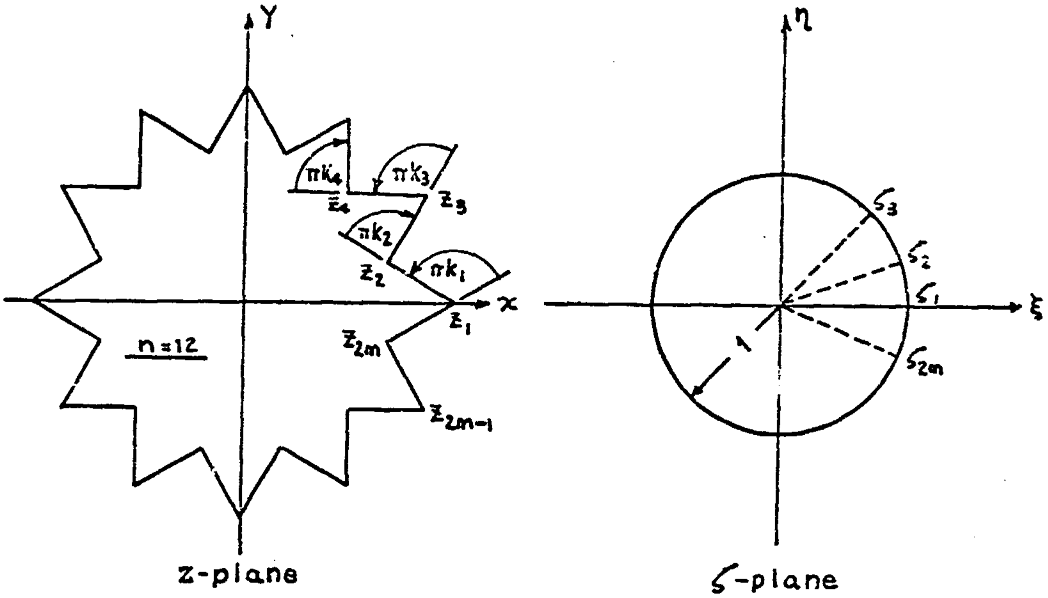

Fig. 1 Mapping of a regular star-shaped polygon onto a unit circle.

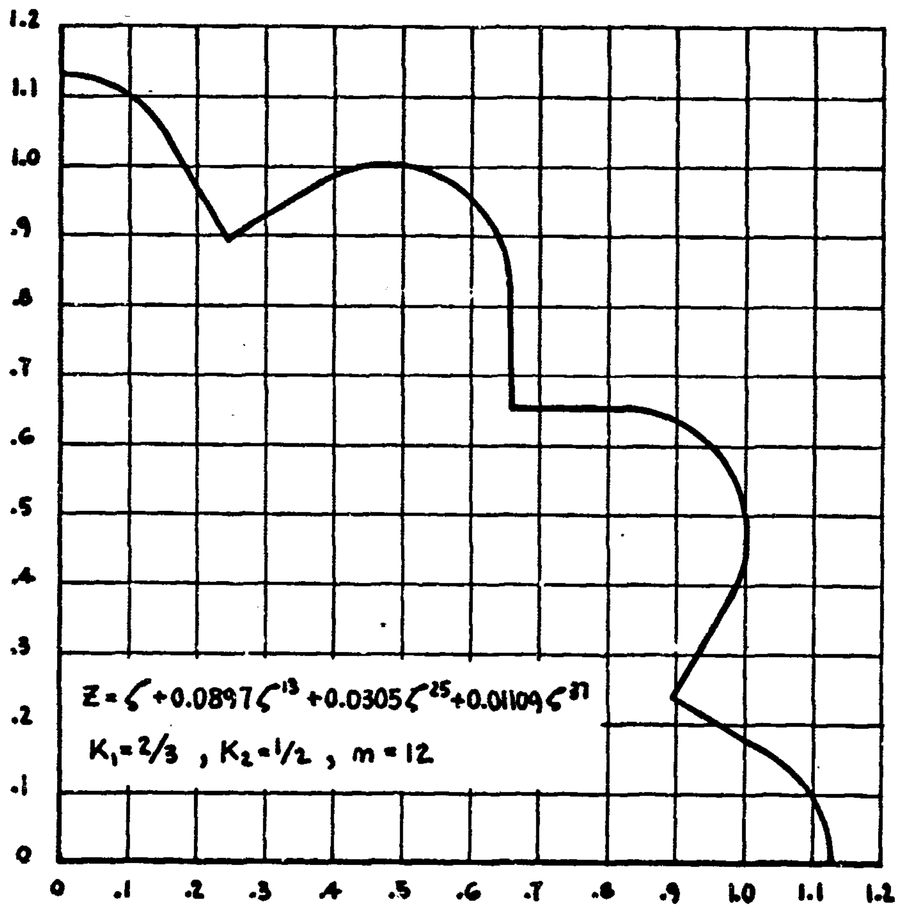

Fig. 2 Region mapped by a four-term polynomial.

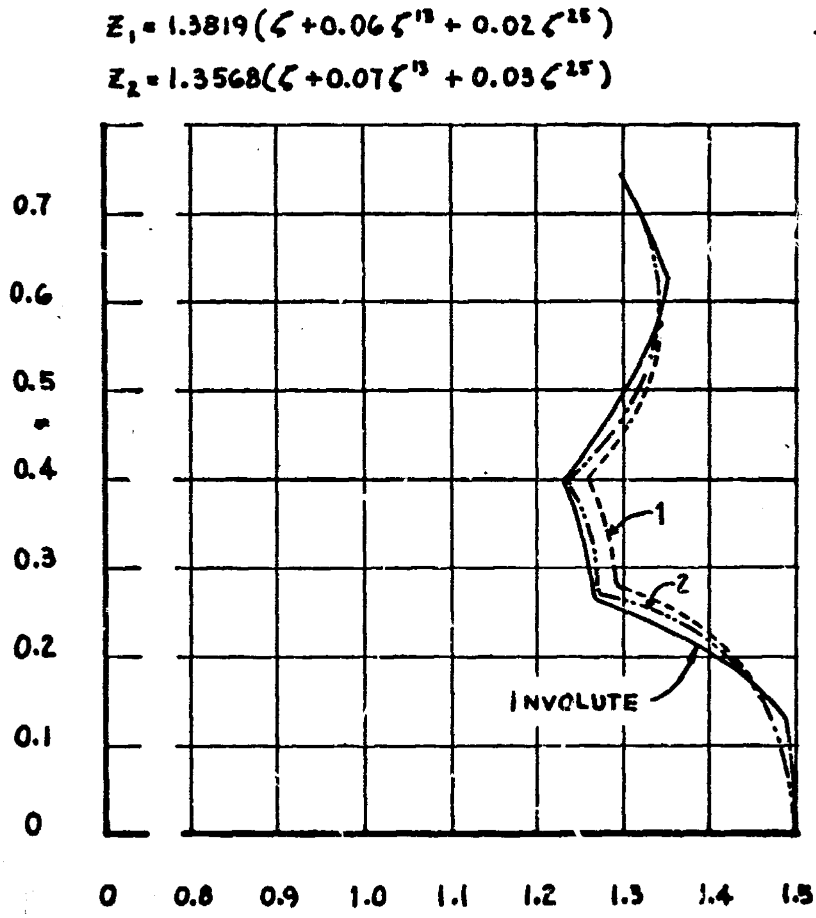

Fig. 3 Mapping of involute spline.

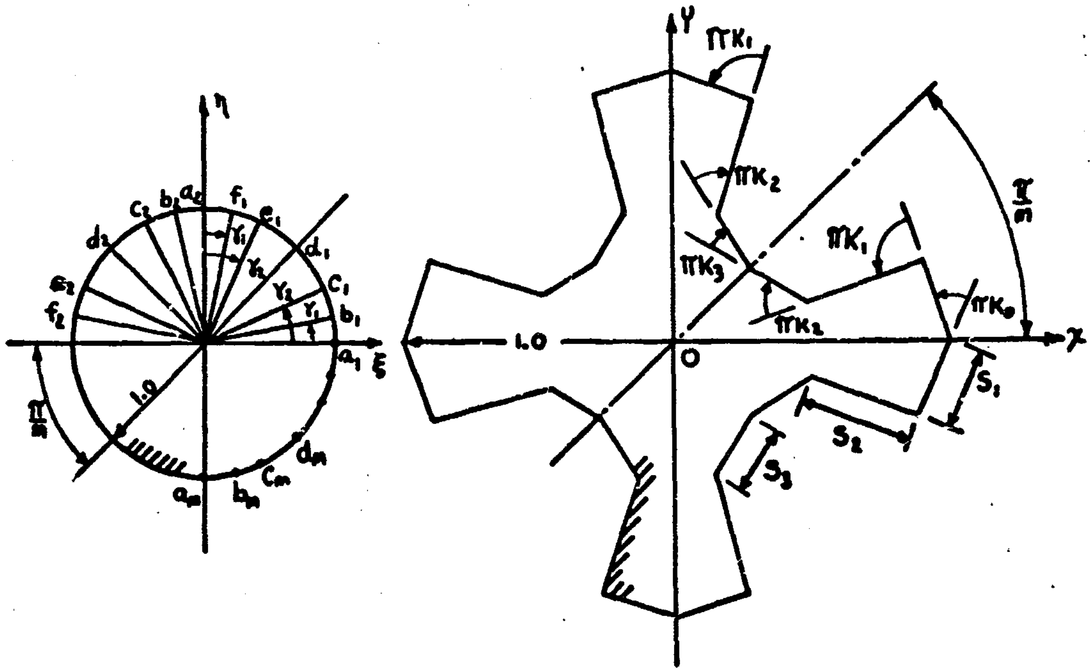

Unit Circle on ζ-plane

Polygon on z-plane

Fig. 4 Mapping of a polygonal star; n = number of star points, positive πK_j is counterclockwise.

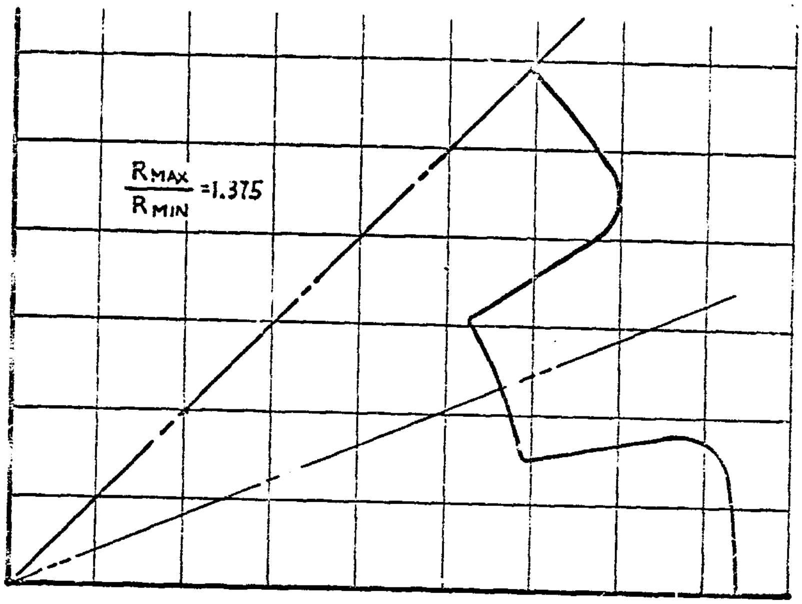

Fig. 5 Map of 8 Notch Spline Shaft

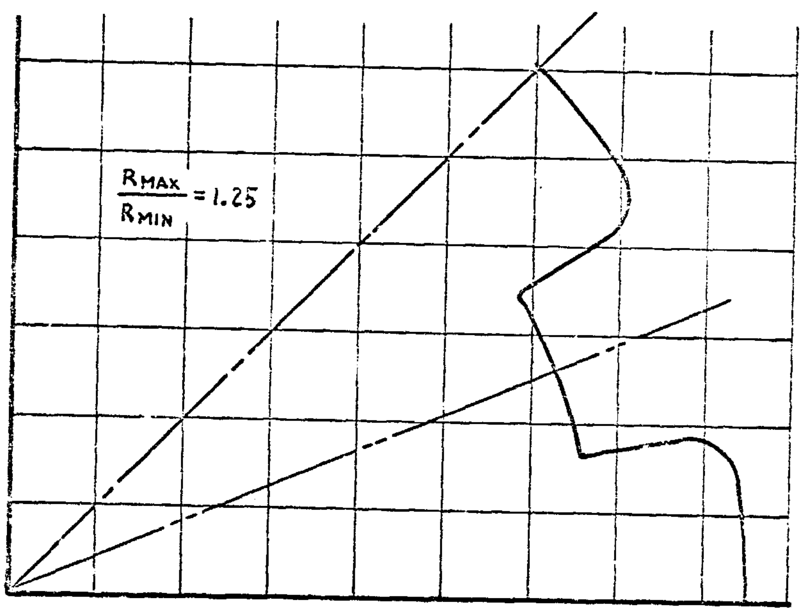

Fig. 6 Map of 8 Notch Spline Shaft

Lines of Constant Shear Stress, τ, in Terms of Torque, T

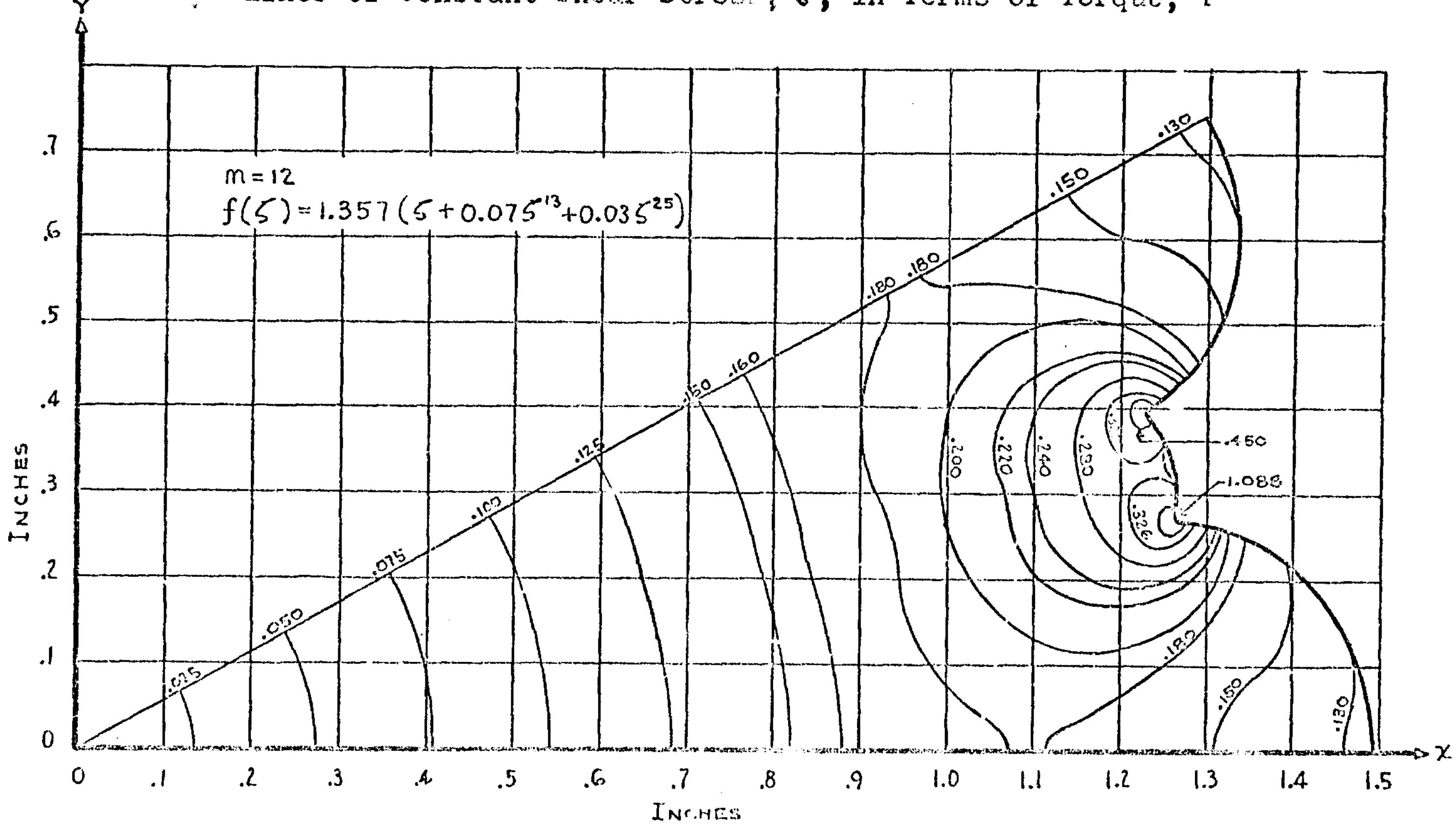

Fig. 7 Distribution of Shear Stress

References

1. Kantorovich, L. V., and Krylov, V. I., "Approximate Methods of Higher Analysis," P. Noordhoff, Groningen, The Netherlands, 1958, p. 474.

2. Ibid., p. 451.

3. Higgins, T. J., "An epitomization of the basic theory of the generalized Schwarz-Christoffel transformation as used in applied physics," Journal of Applied Physics, 22, 3, 1951, pp. 365-366.

4. Nehari, Z., "Conformal Mapping," First Edition, McGraw-Hill Book Company, New York, 1952, p. 192.

5. Stevenson, A. C., "The torsion of a fluted column," Philos. Magazine, Ser. 7, 34, 1943, pp. 115-120.

6. Wittrick, W. H., "Some simple transformation functions for square and triangular holes with rounded corners," Aero. Quart., 11, 1, 1960, pp. 159-199

7. Rim, K., and Stafford, R. O., "Derivation of mapping functions for star-shaped regions," NASA CR-192, NASA, Washington, D. C., 1965, pp. 9-10.

8. Muskhelishvili, N. I., "Some Basic Problems of the Mathematical Theory of Elasticity," P. Noordhoff, Groningen, Holland, 1953, pp. 576-579.

9. Wang, Chi-Teh, "Applied Elasticity," McGraw-Hill Book Co., New York, 1953, pp. 178-181.

10. Hetényi, Miklós, "Handbook of Experimental Stress Analysis," John Wiley and Sons, New York, 1950, pp. 700-751.

11. Bieberbach, L., "Conformal Mapping," Fourth Edition, Chelsea Publishing Co., New York, 1953, p. 128.

12. Okubo, H., "Torsion of a circular shaft with a number of longitudinal notches," Journal of Applied Mechanics, 17, Trans. ASME, 72, 1950, pp. 359-362.

13. Nakazawa, H., "Torsion of a shaft which has a number of longitudinal notches on outer and inner boundary," Proceedings, First Japan National Congress for Applied Mechanics, 1951, pp. 209-214.